ELSEVIER

Chemical Geology 243 (2007) 255–274

CHEMICAL GEOLOGY
INCLUDING
ISOTOPE GEOSCIENCE

www.elsevier.com/locate/chemgeo

Alkali elements (Na, K, Rb) and alkaline earth elements (Mg, Ca, Sr, Ba) in the anoxic brine of Orca Basin, northern Gulf of Mexico

Johan Schijf *

College of Marine Science, University of South Florida, 140 7th Avenue South, St. Petersburg, Florida 33701, USA

Received 6 March 2007; received in revised form 11 June 2007; accepted 11 June 2007

Editor: D. Rickard

Abstract

A profile of filtered seawater and brine samples was collected in the summer of 2003 from a depth of 1500 m down to the bottom of the anoxic, hypersaline Orca Basin (northern Gulf of Mexico). Using ion chromatography and inductively coupled plasma mass spectrometry (ICP-MS), these samples were analyzed for alkali cations (Na^+, K^+, Rb^+), alkaline earth cations (Mg^{2+}, Ca^{2+}, Sr^{2+}, Ba^{2+}), and the major anions chloride (Cl^-) and sulfate (SO_4^{2-}). Major ion concentrations in the brine are consistent with previous studies, confirming that Na plus Cl make up more than 95% of its composition, hence governing its density and hydrodynamic stability. Binary mixing plots across the interface between deep Gulf of Mexico seawater and the anoxic brine are generally linear, but display substantial deviations from conservative behavior at the steepest part of the pycnocline for all analytes except Na, Cl, and Ca. Negative deviations signify localized cation removal by an adsorption or ion-exchange process, probably associated with the dense layers of particles that are trapped there. Especially strong Mg removal may be indicative of dolomitization, whereby the concomitant release of Ca counters its adsorption, resulting in zero net Ca removal. A positive deviation for sulfate is attributed to bacterial sulfide oxidation.

Concentrations of Rb, Sr, and Ba in the homogeneous brine, reported here for the first time, are enriched by factors of 1.5, 1.4, and ~9, respectively, with respect to the overlying seawater. Unlike Ca and Sr, Ba concentrations in the brine are clearly controlled by the solubility of its sulfate salt (barite), causing a maximum of 670 nmol/kg at the interface. Several independent lines of evidence suggest that the brine is formed outside the basin, most likely by the interaction of seawater with regionally extensive evaporite deposits. A simple mass balance shows that the dissolution of about 280 g of halite per kg of seawater can account for the extreme concentrations of Na and Cl in the Orca Basin brine. The same mass balance was applied to a number of minor constituents (K, Rb, Mg, Ca, Sr, SO_4, Br, total iodine) in order to calculate what abundances in the halite are required to reproduce their concentrations in the brine as measured in the present work and by others. The results are entirely compatible with the composition of the Jurassic Louann Salt, specifically with the median of compositions published for a transect spanning early to late stage halites. Elevated abundances of K and Rb point to contributions from bittern facies modified by prior diagenetic contact with seawater.
© 2007 Elsevier B.V. All rights reserved.

Keywords: Orca Basin; Hypersaline; Anoxic; Alkali elements; Alkaline earth elements; Evaporite

1. Introduction

Submarine anoxic brine pools are undoubtedly among the most chemically exotic oceanic environments

* Present address: Chesapeake Biological Laboratory, University of Maryland Center for Environmental Science, P.O. Box 38, Solomons, Maryland, USA. Tel.: +1 410 3267387; fax: +1 410 3267341.
E-mail address: schijf@cbl.umces.edu.

0009-2541/$ - see front matter © 2007 Elsevier B.V. All rights reserved.
doi:10.1016/j.chemgeo.2007.06.011

known. They are created by processes that deform the seafloor, exposing ancient evaporite deposits to ambient seawater and simultaneously excavating a deep basin to hold the resulting hypersaline solution. Such a coincidence of circumstances is rare and has only been encountered and studied in a handful of locations, including geothermal brines in the Red Sea (Swallow and Crease, 1965; Backer and Schoell, 1972), the cold brines of the Tyro, Bannock, Urania, L'Atalante, and Discovery Basins in the eastern Mediterranean Sea (Jongsma et al., 1983; Scientific staff of Cruise *Bannock* 1984-12, 1985; MEDRIFF Consortium, 1995), and the solitary cold brine of the Orca Basin in the northern Gulf of Mexico (Shokes et al., 1977).

The extreme salinity of these brines gives rise to a pronounced density gradient, or pycnocline, severely restricting the free exchange of water and solutes across the interface with the overlying seawater (de Lange et al., 1990c). As biogenic particles continue to rain onto the brine from the euphotic zone, organic matter is bacterially remineralized, causing depletion of oxygen followed by a gradual build-up of dissolved sulfide. Because of the tremendous hydrodynamic stability and consequent longevity of such a system, this process eventually renders the brine fully anoxic. The concomitant shift in redox potential converts many elements to their most reduced, often more soluble forms. The brines are therefore typically highly enriched in dissolved iron and manganese (Brewer and Spencer, 1969; Trefry et al., 1984) as well as in various trace metals that readily adsorb onto reactive iron and manganese oxyhydroxide surfaces but are released as these carriers reductively decompose in the anoxic water (Schijf et al., 1995). In addition, the concentrations of certain elements may be buffered by the solubility of precipitates whose formation in the open ocean is thermodynamically or kinetically unfavorable, namely transition metal sulfides (Saager et al., 1993), alkaline earth sulfates (Krumgalz et al., 1999), and dolomite (de Lange et al., 1990a). This exceptional array of physical and chemical processes also affects the underlying sediments, which may be characterized by intricate lamination due to the absence of bioturbation and bottom currents, prolonged preservation of microfossils and plant debris (Sheu and Presley, 1986b), elevated contents of organic matter and iron sulfides (the latter imparting a distinctive jet-black color), or the conspicuous presence of normally uncommon minerals like gypsum (Scientific staff of Cruise *Bannock* 1984-12, 1985) and hematite (Sheu and Presley, 1986a).

The Orca Basin, discovered in 1975–76, is located on the continental slope of the northern Gulf of Mexico, centered at 26°55′ N 91°20′ W (Shokes et al., 1977). Whereas similar intraslope depressions are found throughout this area of active salt diapirism, Orca Basin appears to be the only one that contains anoxic brine (Trabant and Presley, 1978). The brine pool, with an estimated total volume of ~5 km^3, only partially fills the basin which covers about 400 km^2. Orca Basin is roughly J-shaped, consisting of two interconnected sub-basins separated by a saddle, a small one to the north and a much larger one to the south. Maximum depth in each of the two sub-basins is at least 2400 m. The vertical extent of the brine layer at these deepest points is approximately 200 m. Based on ^{14}C dating of a sudden transition from gray sediments (assumed to have been deposited in an oxygenated environment) to black ones in a long piston core taken near the center of the saddle, Addy and Behrens (1980) put the beginning of brine emplacement around 8000 years BP. Downward decreasing salinity in the sediment pore waters indicates that the brine did not originate beneath the Orca Basin, but was introduced from somewhere outside. This was confirmed by seismic evidence for salt exposure on the seafloor to the north and southeast (Addy and Behrens, 1980) and by the discovery of a 'brine river', flowing into Orca Basin from the upper slope (Brooks et al., 1990). Addy and Behrens (1980) noted that the level of the brine is below the sill and that accumulation may thus be ongoing. Geochemical studies of the Orca Basin have shown that the composition of the brine with respect to a number of components (Na^+, Cl^-, Br^-, SO_4^{2-}, Ar) is compatible with the dissolution, in ambient seawater, of ~300 g/L of halite from a regionally extensive evaporite deposit known as the Louann Salt (Sheu, 1990).

In this work I present data from a new series of filtered water samples that were collected in the summer of 2003 and span the complete transition from deep Gulf of Mexico seawater to homogeneous brine at high resolution. Precise measurements of major ion concentrations by ion chromatography confirm the dominance of Na plus Cl in the brine and their effect on its physical properties. The use of inductively coupled plasma mass spectrometry (ICP-MS) enabled the first reported analyses of Rb, Sr, and Ba. Simple mass balances, binary mixing plots, and solubility calculations are employed to investigate the source of the brine, while striving to explain observed deviations from conservative behavior at the seawater–brine interface in terms of redox–chemical processes, enhanced scavenging within the dense layers of particles trapped by the pycnocline, and the potential precipitation of alkaline earth sulfates (barite) and carbonates (dolomite) occurring both at the interface and within the brine itself.

2. Materials and methods

2.1. Sample collection

Orca Basin was sampled from R/V *Longhorn* (University of Texas Marine Science Center) in June of 2003. Seawater and brine samples were collected during multiple CTD/Rosette casts, using cleaned 12-L Niskin bottles fitted with silicone internal springs. Samples were drawn on deck straight into acid-washed 1-L Teflon bottles, which were capped with minimal headspace and quickly placed in a glovebag (Model X-27-17; I^2R – Instruments for Research and Industry, Cheltenham, PA) inside the shipboard laboratory. All subsequent sample preparation was performed under inert atmosphere by flushing the glovebag with a continuous stream of filtered, high-purity nitrogen gas. This precaution generally ensures trace metal-clean conditions and particularly prevents rapid oxidation of Fe(II) in the anoxic brine samples, which would lead to precipitation of ferric hydroxides and collateral scavenging of many other elements. Shortly after collection, seawater and brine samples were vacuum-filtered through Millipore (Bedford, MA) Steritop filter units (150 mL, 73 mm GV Durapore membrane, 0.22-μm pore size), using a small electric air pump on a rheostat, both kept outside the glovebag. The filter units were screwed directly onto an acid-washed 125-mL Teflon wide-mouth bottle and each 1-L sample was filtered in eight 125-mL aliquots. Two aliquots were used to rinse one acid-washed 250-mL Teflon and one acid-washed 250-mL PE bottle. Each bottle was then filled with two aliquots of filtered sample and acidified with 250 μL of TraceMetal grade concentrated HNO_3 (Fisher Scientific, Pittsburgh, PA). The final two aliquots were discarded. The cover of the Steritop reservoir was replaced and secured with tape and the entire unit stored in a shipboard freezer and later transferred to a shore laboratory freezer for future analysis of particulate metal concentrations. The bottles with the filtered, acidified samples were tightly capped and stored in ziploc bags for transport to the shore laboratory.

2.2. Sample analysis by ion chromatography (IC) and ICP-MS

Further sample handling and preparation were performed inside a class-100 clean air laboratory or laminar flow bench. Trace metal grade reagents were prepared with water from a Millipore purification system (Milli-Q water). Approximate densities of the seawater and brine samples were determined by weighing 25-mL aliquots in Pyrex class-A volumetric flasks on a Mettler Toledo (Columbus, OH) AB104-S analytical balance. Temperature and relative humidity were monitored during each series of weighings and found to be constant at 21 °C and 55%, respectively. A set of three flasks was used and their tare weights were determined separately before every series. After each weighing, the volumetric flask was rinsed with Milli-Q water and dried in the laminar flow bench, but not re-tared. Sample weights were calculated by subtracting the tare weights from the corresponding total weights. With the same method and under similar conditions, the density of Milli-Q water was determined to be 0.9984 kg/dm^3, which may be compared with its actual density at 21 °C and 1 atm: 0.9979925 kg/dm^3 (Kell, 1975). Some sample densities are the average of 4 or 5 replicate weighings. Based on these observations the absolute accuracy and precision of the measurement are estimated as ±0.0005 kg/dm^3.

A total of 14 filtered, acidified seawater and brine samples was analyzed for major cations (Na^+, K^+, Mg^{2+}, Ca^{2+}) and anions (Cl^-, SO_4^{2-}) with a Dionex (Sunnyvale, CA) DX-500 IC, as outlined in detail by Schijf and Byrne (2007). Briefly, a series of 6 or 8 dilutions was prepared from each sample with Milli-Q water, using dilution factors (by volume) of 100–40,000 depending on the analyte and its concentration in specific samples. Analyte concentrations were determined from the intercept of a linear regression of the logarithm of the concentration of all dilutions within a series plotted as a function of the logarithm of the dilution factor, setting the slope to its theoretical value of −1. Due to the non-seawater-like composition of the brine samples, some dilutions could not be used in all regressions, either because their concentrations were too close to the detection limit or too far beyond the calibrated concentration range. The extreme levels of Na and Cl in the brine necessitated the removal of Cl from the most concentrated dilutions with Dionex OnGuard® II Ag cartridges, to allow proper analysis of SO_4^{2-} (see also Schijf and Byrne, 2004). No cartridges are available for the selective removal of Na and this may have decreased the accuracy of K concentrations in the brine. A standard reference material (SRM) was analyzed eleven times during various IC runs to validate the cation calibrations (SLRS-4 River Water Reference Material for Trace Metals, National Research Council Canada). As observed before, analytical recoveries for this SRM were somewhat low, about (95±3)% for K and Mg, and about (90±3)% for Na and Ca. However, as also observed before, the average recovery for independent check samples prepared from single-element IC standards (VHG Labs, Manchester, NH) was (102±2)% for all

six ions. This suggests that the low cation recovery is peculiar to SLRS-4 and probably results from its acidity (pH 1.6), which is known to affect IC analysis but not the FAAS and ICP-AES techniques that were used in the SRM's certification. Analytical uncertainty, based on check sample recoveries and replicate samples, is 1–2% for all six ions, after removal of systematic outliers (Schijf and Byrne, 2007), although Na interference may have caused K concentrations in the brine to be slightly overestimated.

Seawater and brine samples were analyzed for Rb, Sr, and Ba with an Agilent 4500 Series 2 inductively coupled plasma mass spectrometer (ICP-MS), again using a modification of the method described by Schijf and Byrne (2007). Seawater samples were diluted 100-fold and brine samples 200-fold with 1% HNO_3 and spiked with 20 ppb Y and 10 ppb Cs, acting as internal standards. At these dilutions, signal suppression induced by the sample matrix is stable and within acceptable limits (Schijf and Byrne, 2007). Concentrations were determined by external calibration with one blank and four mixed standard solutions. The highest standard contained 2 ppb Rb, 100 ppb Sr, and 0.5 ppb Ba. Rb was recorded at mass 85 and Sr at mass 88 (they interfere at mass 87), while Ba was recorded at mass 137 and 138. Rb and Sr were normalized to Y and the Ba isotopes to Cs. Preliminary semi-quantitative analyses of the brine samples were performed to assure that natural Y, Cs, La, and Ce concentrations were low enough to prevent significant deviations from the intended internal standard concentrations, as well as isobaric interference at mass 138. Saltwater SRMs available at USF (CASS-4 and SLEW-3, National Research Council Canada) are not certified for Rb, Sr, and Ba. The ICP-MS method was therefore validated with the river water SRM SLRS-4 (Sr and Ba only) and two USGS SRMs (PPREE1 and SCREE1), metal-contaminated acid mine waters that are specifically certified for the rare earth elements but have also been tested for a host of other elements, including Rb, Sr, Y, Ba, and Cs (Verplanck et al., 2001). These three SRMs have low ionic strengths, yet dilution by a factor of 10–50 was still required to bring analyte concentrations within range of the calibration lines. PPREE1 and SCREE1 are highly enriched in the internal standard element Y hence appropriate corrections were made based on its estimated concentrations (Verplanck et al., 2001). All measurements were within the reported 95% confidence limits of the expected concentrations, except for Rb and Sr in SCREE1, which yielded analytical recoveries of 106%. After dilution, this SRM had the highest native Y concentration and thus required the largest correction. Based on these results and replicate analyses of every sample ($n=6$–9), accuracy and precision of the ICP-MS method are estimated to be <1% for Rb and Sr, and ~3% for Ba for both seawater and brine.

3. Results

Table 1 gives an overview of the 14 seawater and brine samples collected from R/V *Longhorn* on 8–16 June 2003, including uncorrected CTD-recorded depths,

Table 1
Orca Basin seawater and brine samples collected from R/V *Longhorn* in June of 2003

Depth (m)	Hydrocast #	Niskin #	Date	Location [a]	Sample	Density (d) (kg/dm^3)	$1000\times(d-d_0)$ (g/dm^3)
1500	16	4	06/16/03	26°54.10 N 91°21.11 W	Seawater	1.0243	25.86
2150	13	3	06/13/03	26°54.77 N 91°24.38 W	Seawater	1.0263	27.91
2175	5	3	06/09/03	26°56.05 N 91°20.75 W	Interface	1.0278	29.41
2190	9	4	06/11/03	26°55.17 N 91°23.33 W	Interface	1.0323	33.86
2200	4	3	06/09/03	26°55.56 N 91°21.74 W	Interface	1.0371	38.68
2210	12	4	06/12/03	26°54.07 N 91°21.50 W	Interface	1.0382	39.77
2220	8	4	06/10/03	26°55.17 N 91°21.82 W	Interface	1.0447	46.28
2235	11	4	06/12/03	26°54.70 N 91°23.71 W	Interface	1.1046	106.2
2240	3	3	06/09/03	26°53.82 N 91°23.80 W	Interface	1.1660	167.6
2250	10	4	06/11/03	26°55.34 N 91°22.18 W	Brine	1.1899	191.5
2260	7	4	06/10/03	26°55.59 N 91°22.76 W	Seawater [b]	–	–
2280	2	4	06/08/03	26°54.22 N 91°21.21 W	Brine	1.1913	192.9
2295	6	4	06/10/03	26°55.51 N 91°23.46 W	Brine	1.1903	191.9
2460	16	2 [c]	06/16/03	26°54.07 N 91°21.03 W	Brine	1.1914	193.0

See text for a detailed description of sampling methods. Density was determined gravimetrically at $T=21$ °C and 55% relative humidity. Density of Milli-Q water (d_0) was determined to be 0.9984 kg/dm^3 under the same conditions. Uncertainty in the density measurements is estimated as ±0.0005 kg/dm^3.

[a] Coordinates were recorded when the Niskin bottle was tripped.

[b] Low density and solute concentrations indicate a delayed trip of the Niskin bottle; this sample was excluded from further analysis.

[c] This Niskin bottle had a nylon-coated stainless steel internal spring.

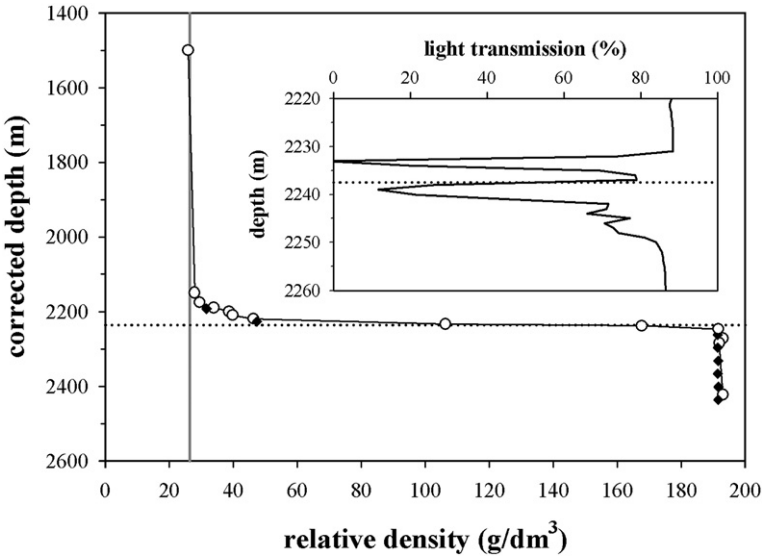

Fig. 1. Relative density ($1000\times(d-d_0)$; T=21 °C) of the Orca Basin brine and overlying seawater. Diamonds are data (T=25 °C) from Millero et al. (1979). Sample depths were corrected as described in the text. The vertical grey line represents the relative density of standard seawater (S=35.00). The inset enlarges a detail of the interface for a typical light transmission profile (hydrocast 11, 12 June 2003), revealing two dense particle layers straddling the pycnocline. The vertical axis of the inset shows CTD-recorded (uncorrected) depth. Horizontal dotted lines indicate the position of the steepest part of the pycnocline on each depth scale.

hydrocast and Niskin bottle numbers, and GPS locations taken when the Niskin bottle was tripped. Niskin bottles 3 and 4 were fitted with silicone internal springs for trace metal-clean sample collection. During hydrocast 16, Niskin bottle 3 failed and the 2460 m sample was taken instead from Niskin bottle 2, which had a Nylon-coated stainless steel internal spring. While this may affect dissolved trace metal concentrations, analyses of the elements discussed here do not appear to be compromised.

Also given in Table 1 are sample densities, measured gravimetrically at T=21 °C and 55% relative humidity, and relative densities, defined by Millero et al. (1979) as $1000\times(d-d_0)$, where d_0 is the density of pure water measured under the same conditions. A profile of relative density, illustrating the vertical structure of the Orca

Table 2
Concentrations of alkali elements, alkaline earth elements, and major anions in Orca Basin below 1500 m

Depth (m)	$[Na^+]$	$[K^+]$	$[Rb^+]$	$[Mg^{2+}]$	$[Ca^{2+}]$	$[Sr^{2+}]$	$[Ba^{2+}]$	$[Cl^-]$	$[SO_4^{2-}]$
Seawater	469	10.2	1.4	52.8	10.4	89	–	549	28.2
1500	468±1	10.3±0.1	1.31±0.01	52.6±0.3	10.6±0.1	86.9±0.8	62±2	535±9	27.5±0.1
2150	502±1	10.4±0.1	1.31±0.01	52.3±0.4	10.6±0.1	87.0±0.5	81±2	549±5	27.2±0.3
2175	541±7	10.4±0.2	1.34±0.01	50.8±0.5	10.7±0.2	88.0±0.2	111±2	614±8	27.9±0.1
2190	657±1	10.9±0.1	1.35±0.01	51.8±0.2	11.5±0.1	88.7±1.0	165±5	717±7	28.1±0.2
2200	756±2	11.1±0.2	1.37±0.01	52.0±0.2	12.0±0.1	89.8±0.5	211±5	803±11	28.3±0.1
2210	790±2	11.0±0.2	1.37±0.01	52.1±0.4	12.2±0.1	90.3±0.5	223±6	847±10	28.4±0.1
2220	919±4	11.1±0.1	1.40±0.02	51.5±0.4	12.7±0.2	91.6±0.5	273±6	959±12	28.3±0.2
2235	2289±35	12.4±0.1	1.49±0.01	38.5±0.4	18.6±0.3	97.5±0.5	670±16	2317±26	39.6±0.3
2240	3630±28	15.1±0.2	1.76±0.02	38.3±0.4	25.0±0.2	113±1	590±17	3616±23	39.4±0.5
2250	4133±61	17.1±0.2	1.92±0.01	41.0±0.6	26.7±0.6	122±0.4	556±13	4148±53	39.0±0.5
2280	4178±57	17.9±0.4	1.94±0.01	41.3±0.5	26.5±0.3	121±1	545±10	4160±25	38.4±0.5
2295	4155±48	17.7±0.2	1.94±0.01	41.1±0.3	26.6±0.3	121±1	550±15	4157±45	38.8±0.3
2460	4155±47	17.4±0.1	1.95±0.01	40.9±0.3	26.5±0.3	122±1	545±12	4080±50	38.7±0.3

All concentrations in mmol/kg, except Rb and Sr in μmol/kg and Ba in nmol/kg. Rb, Sr, and Ba concentrations are the average of 6–9 replicates±one standard deviation. Other concentrations and uncertainties were determined from linear regressions of 6 or 8 sample dilutions (see text). The brine appears compositionally homogeneous below ~2250 m. Seawater composition (S=35.00) after Byrne (2002).

Table 3
Average composition of the brine compared with values from the literature

Element	This work	Shokes et al. (1977)	Millero et al. (1979)	Van Cappellen et al. (1998)
$[Na^+]$	4155±18	3980	4141	4240
$[K^+]$	17.5±0.3	16.1	16.1	17.0
$[Rb^+]$	1.94±0.02	–	–	–
$[Mg^{2+}]$	41.0±0.2	43.2	43.2	42.4
$[Ca^{2+}]$	26.6±0.1	27.2	27.2	29.0
$[Sr^{2+}]$	121±0.3	–	–	–
$[Ba^{2+}]$	549±5	–	–	–
$[Cl^-]$	4136±38	4217	4217	4450
$[SO_4^{2-}]$	38.7±0.3	38.1	38.1	29.0 [a]

Each value in the second column is the mean of the four deepest samples±one standard deviation (see Table 2). All concentrations in mmol/kg, except Rb and Sr in μmol/kg and Ba in nmol/kg.

[a] The sulfate concentration of Van Cappellen et al. (1998) appears in error; since it is identical to their Ca concentration, it is probably a misprint.

Basin water column, is drawn in Fig. 1. The two shallowest samples (1500 and 2150 m) both have the density of seawater. The four deepest samples have ~20% higher densities and appear to represent a homogeneous layer of brine. The aforementioned samples are identified in Table 1 as "seawater" and "brine", respectively. Seven samples in between these end members have intermediate, downward increasing densities and are identified as "interface". The 2260 m sample, ostensibly within the homogeneous brine, was found to have a seawater-like density. This is probably due to a delayed trip of the Niskin bottle during the upcast, causing the sample to be collected at a much shallower depth than intended. That sample was excluded from further analysis. The 2235 and 2240 m samples constitute the steepest part of the pycnocline (Fig. 1) and are labeled in all subsequent figures with closed symbols.

Concentrations of Na, K, Mg, Ca, and the anions chloride and sulfate, measured by ion chromatography, as well as concentrations of Rb, Sr, and Ba, measured by ICP-MS, are presented in Table 2 together with the composition of standard seawater (S=35.00) for comparison. All concentrations were converted to units of mol/kg, using the densities in Table 1. Profiles are drawn in Figs. 3, 4 and 7. Once again the four deepest samples represent homogeneous brine as they have nearly identical concentrations. The mean composition of these four samples is listed in Table 3, along with three data sets from the literature.

In Fig. 2 it is demonstrated that Cl shows excellent linear correlations with density and with Na throughout the sampled part of the Orca Basin water column. Analogously, the other solutes were tested for conservative behavior by means of binary mixing plots (Figs. 3, 5 and 7). For analytical reasons (Schijf and Byrne, 2007), cation behavior was assessed by comparison with Na and sulfate behavior by comparison with Cl. All but one of the correlations are linear, indicating conservative mixing of brine and seawater at all depths with the exception of 2235 and 2240 m i.e., the steepest part of the pycnocline. Distinct negative deviations from linearity are noted there for K, Rb, Mg, Sr, and a positive deviation for sulfate. Such behavior is generally interpreted as signifying removal, respectively release of the corresponding solutes at those depths. Interestingly, the Ca–Na mixing plot (Fig. 5) is entirely linear, with little evidence of Ca removal or release anywhere. In contrast, the Ba–Na mixing plot (Fig. 5) is only linear above the seawater–brine interface, deviating very strongly from

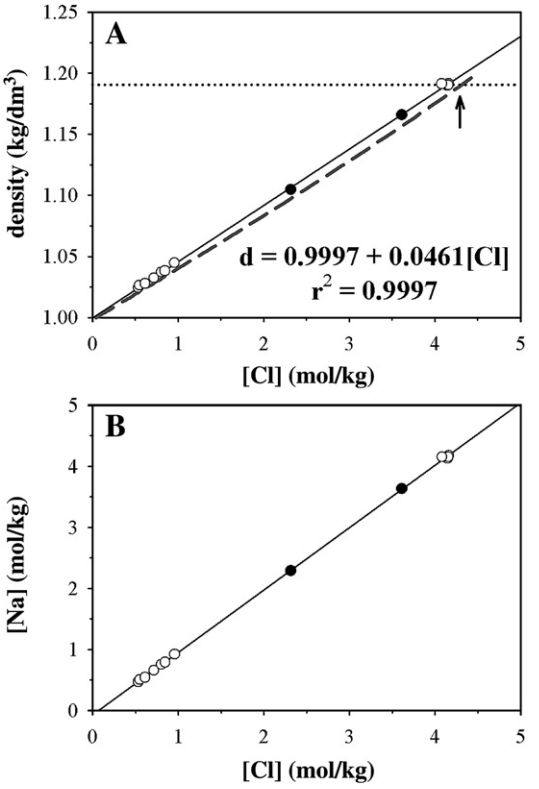

Fig. 2. (A) Density (d) as a function of the Cl concentration. Two samples at the steepest part of the pycnocline are labeled with closed symbols. Linear regression includes all data. The dashed gray curve delineates the density of aqueous Na–Cl solutions at T=20 °C (Weast and Astle, 1982). Good agreement confirms that the density of the brine is governed by its predominant Na–Cl composition (~5 M). The horizontal dotted line is the average density of the brine. The arrow indicates the Cl concentration of an Na–Cl solution with the same absolute salinity as the brine (S=250.8). (B) Na concentration as a function of the Cl concentration.

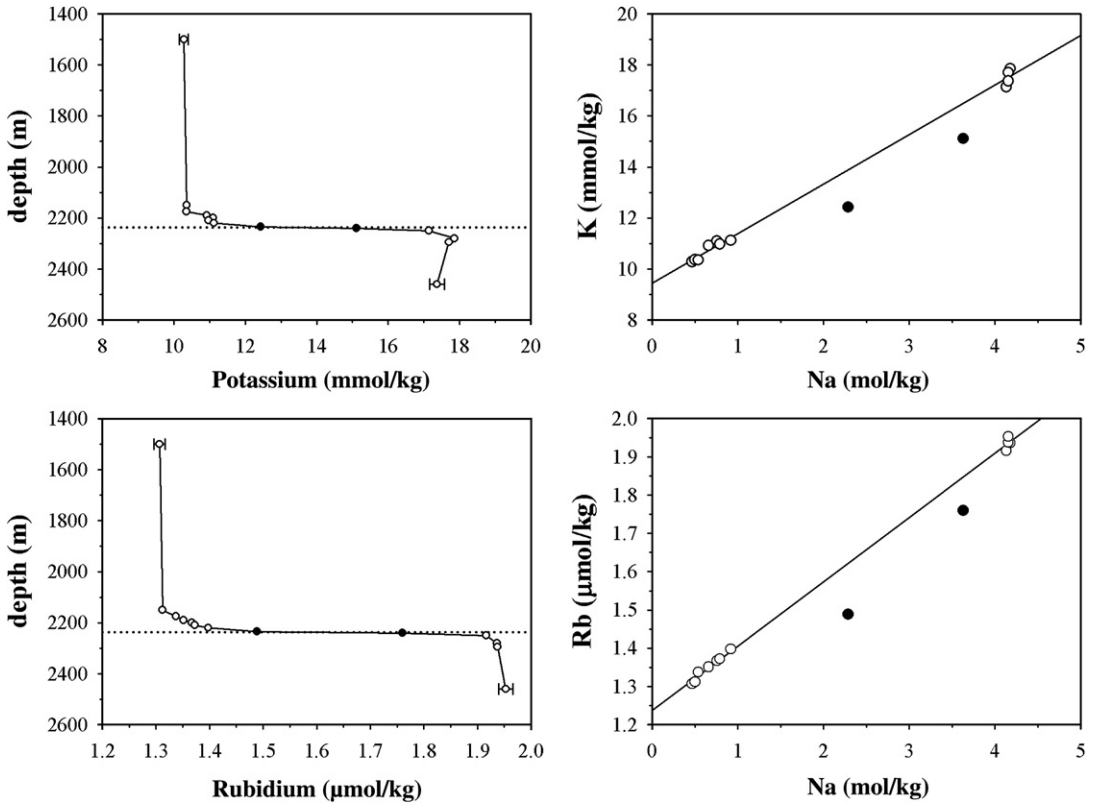

Fig. 3. Profiles of the dissolved alkali elements potassium (K) and rubidium (Rb), and the corresponding K–Na and Rb–Na mixing plots. Error bars on the shallowest and deepest samples are representative of analytical uncertainties for the seawater and brine samples, respectively. Horizontal dotted lines indicate the steepest part of the pycnocline. Closed symbols mark the same samples as in Fig. 2. Linear regressions are through the open symbols only. Note the strong deviations at the interface from otherwise conservative mixing of seawater and brine.

2235 m down to the bottom. The Ba profile (Fig. 4) has a maximum at 2235 m, yet below this depth Ba concentrations decrease to levels that are almost 20% lower. This is probably due to buffering of the Ba concentration by precipitation of barite. The following discussion presents a more quantitative interpretation of these results in terms of physical and chemical processes operating at the interface and within the brine itself.

4. Discussion

4.1. Na and Cl concentrations and the stability of the pycnocline

In Fig. 1 relative densities are compared with data of Millero et al. (1979). First, a brief discussion of depth scales is in order. The uncorrected CTD-recorded depths in Table 1 (pressure readings) were converted to actual depths by adjusting for the cumulative excess weight of the overlying brine. Each layer bounded by two consecutive samples was corrected with the average of the densities at the top and bottom of that layer. Since the correction is an approximation and was made strictly for the purpose of this comparison, I will continue to use uncorrected depths throughout the remainder of the discussion and in all subsequent figures. Millero et al. (1979) expressed depth as meters above the seafloor without providing a total depth nor any station information other than that their samples were collected from R/V *Gyre*. Whereas they stated that 245 m above the seafloor equalled a depth of ~2250 m, this yields a total depth of 2495 m, which seems too large. Preliminary data were published two years earlier in an identically titled abstract (Millero et al., 1977) hence the samples of Millero et al. (1979) are presumably from the same 1976 or 1977 R/V *Gyre* cruise as those of Wiesenburg et al. (1985) who did record a total depth. Their value of 2436 m is consistent with the actual depth of my deepest sample (2422 m), which was collected a safe distance above the seafloor to prevent contaminating the Niskin bottles with sediment or damaging the CTD/Rosette. After applying the total depth of Wiesenburg et al.

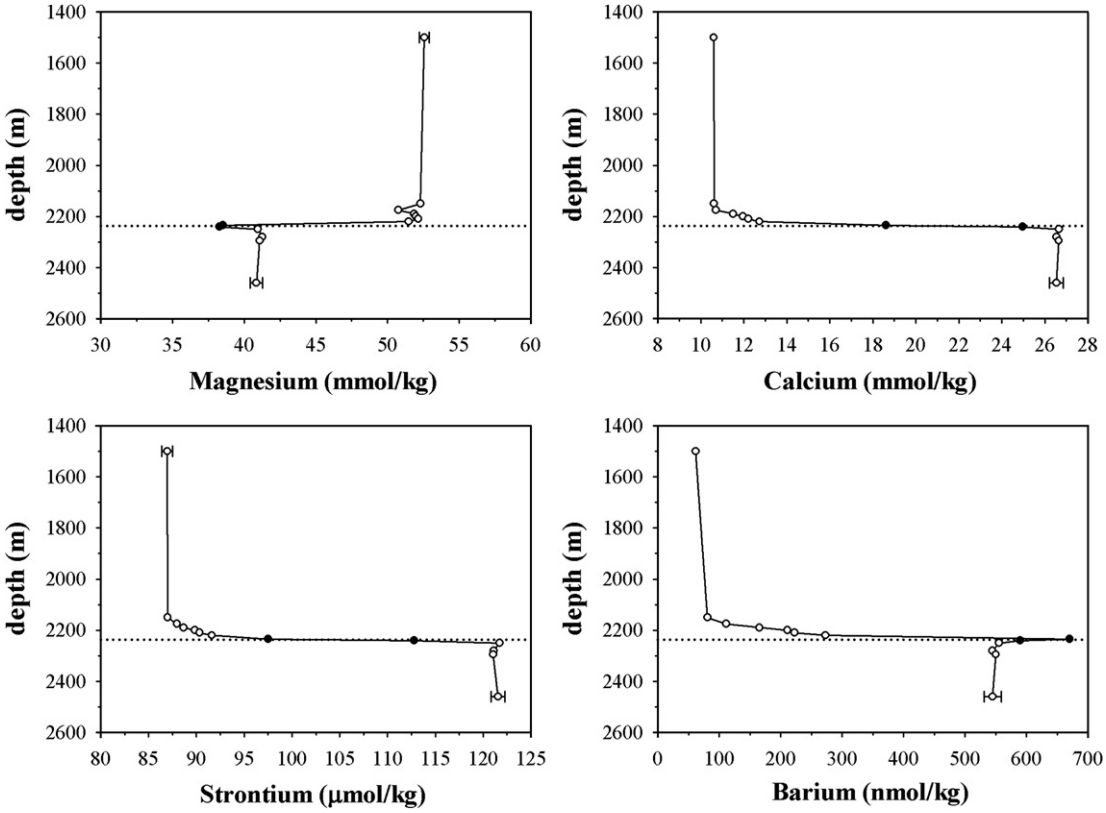

Fig. 4. Profiles of the dissolved alkaline earth elements magnesium (Mg), calcium (Ca), strontium (Sr), and barium (Ba). Error bars on the shallowest and deepest samples are representative of analytical uncertainties for the seawater and brine samples, respectively. Some error bars are within the size of the symbol. Horizontal dotted lines indicate the steepest part of the pycnocline. Closed symbols mark the same samples as in Fig. 2.

(1985) to the data of Millero et al. (1979), the two density profiles were superimposed (Fig. 1). In view of the uncertainties in the depth scales and the temperature difference between the two data sets, agreement is good both within the brine and across the pycnocline.

In Fig. 2A, density is plotted as a function of the Cl concentration, in mol/kg. Millero et al. (1979) fitted their density data as a function of chlorinity (g/kg) to an equation of the form:

$$d = d_0 + A[\mathrm{Cl}] + B[\mathrm{Cl}]^{3/2} + C[\mathrm{Cl}]^2 \quad (1)$$

where d_0 is the density of pure water and A, B, and C are constants. In a similar regression of the data in Fig. 2A several parameters were ill-defined, suggesting that an equivalent degree of complexity is not warranted here. Instead, a linear regression (i.e., omitting the last two terms in Eq. (1)) proved adequate. Standard errors in d_0 and A are 0.0007 and 0.0002, respectively. Combined errors can therefore not fully account for the difference between the value of d_0 derived from the regression and its measured value. This almost certainly reflects a small analytical bias in the Cl concentration, which could be due to non-linearity of the calibration lines or a slow accumulation of blank in the calibration standards (but not in the samples). Also shown in Fig. 2A is the density of aqueous Na–Cl solutions (Weast and Astle, 1982). Millero et al. (1979) concluded that the density of the brine best matches the density of an Na–Cl solution with the same absolute salinity (S=250.8). The Cl concentration of such a solution is indicated in Fig. 2A by an arrow and the density difference at that point (1240 ppm) is remarkably close to the value of 1380 ppm found by Millero et al. (1979). This observation and the correspondence between the two curves in Fig. 2A confirm that the physical properties of the brine, including density, are governed by the concentrations of Na plus Cl, which make up more than 95% of its composition. Minor discrepancies are caused by contributions from the other major ions. Salinity or chlorinity have been considered conservative quantities in geochemical studies of the Red Sea brines (Craig, 1969), the eastern Mediterranean brines (de Lange et al., 1990c), as well as the Orca Basin brine

(Van Cappellen et al., 1998). The linear correlation in Fig. 2A thus establishes that, despite a shift in composition, density can be treated as a conservative quantity in mixtures of seawater and brine. The same pertains to Na, as shown in Fig. 2B. The non-zero offset in the latter case is again attributed to a small analytical bias in the Na or Cl concentration, or both (see also Schijf and Byrne, 2007).

A conspicuous feature of the density profile in Fig. 1 is that the pycnocline does not have the symmetrical, elongated S-shape expected from a one-dimensional advection–diffusion model of solute transport across the interface: it is stretched out above the interface and foreshortened below. The same effect was observed for the Red Sea brines in profiles of Na concentration and temperature by Craig (1969), who remarked that the one-dimensional model predicts downward advection of seawater into the brine, which is quite implausible. As an alternative explanation, he suggested a two-dimensional model wherein solutes supplied via diffusion and upward advection of brine are removed above the interface via horizontal advection, resulting from a convection cell driven by a strong thermal gradient at the seafloor outside the basin. Two arguments render this model unsuitable for the Orca Basin: (i) unlike in the Red Sea deeps, where geothermal heating fuels a temperature gradient of >20 °C at the seawater–brine interface, the Orca Basin brine is only ~1.4 °C warmer than the overlying seawater (Wiesenburg et al., 1985) and thermal convection is probably weak; (ii) unlike the Red Sea brines, the Orca Basin brine does not overflow the sill and horizontal advection along the interface must be considerably restricted by the basin walls.

Craig (1969) assumed constant diffusivity (molecular or turbulent) across the interface, yet the Stokes–Einstein relation dictates that the molecular diffusion constant is inversely proportional to viscosity (Li and Gregory, 1974), which in turn increases with the Na–Cl concentration (Weast and Astle, 1982). Consequently, diffusion out of the interface layer into the overlying seawater is faster than diffusion into the interface layer from the brine below, giving rise to net removal just as horizontal advection would. While a rigorous numerical treatment using a one-dimensional advection–diffusion model with a depth-dependent diffusion constant is outside the scope of this paper, a simple iterative calculation suggests that Fick's Law diffusion can lead to the observed pycnocline shape under such conditions. The effect, albeit subtle, could add up to a persistent asymmetry over the estimated 8000-year age of the brine if steady state is maintained through a minimal rate of upward advection balancing its proposed ongoing accumulation (Addy and Behrens, 1980). On the other hand, several authors have commented upon a pronounced step in the dissolved oxygen profile as evidence for structural anomalies at the interface (Takayanagi and Wong, 1985; Wiesenburg et al., 1985; Wong et al., 1985). It is possible that these characteristics are the remnants of transient events, for example intermittent sediment slumping (Tompkins and Shephard, 1979). Oxygen and temperature anomalies within the broad interface layer of the Black Sea were tied by Konovalov et al. (2003) to pervasive lateral injection of Bosporus plume waters. However, as stated before, horizontal advection is less likely in Orca Basin and continuous temperature profiles (not shown) resemble the density profile (Fig. 1), showing no obvious anomalies of any kind. At the interface of Bannock Basin, whose brine has a comparable estimated age but may be completely stagnant, no asymmetrically shaped pycnocline was found (de Lange et al., 1990c). The disparate origins and histories of the Red Sea, eastern Mediterranean, and Orca Basin brines may well demand a different explanation in each case.

Regardless what mechanism is responsible for the exact shape of the pycnocline, its prodigious stability (Van Cappellen et al., 1998) ensures its efficacy as a particle trap (e.g., Ryan et al., 1969; Trefry et al., 1984). The light transmission profile in Fig. 1 heralds the existence of multiple layers of particles directly above the top of the brine (2220–2250 m). A slight vertical offset between upcast (density) and downcast (light transmission) profiles and the rounding of all CTD-recorded depths to the nearest 5 m (Table 1) obscures the fact that the 2235 and 2240 m samples were taken at the cores of the two densest layers. This was accomplished by tripping the Niskin bottles at depths where the transmissometer showed maximum light absorption. These particle layers will be shown to have a measurable effect on the dissolved concentrations of many solutes, even the relatively chemically inert alkali elements.

4.2. Non-conservative behavior at the seawater–brine interface

The highly linear correlations of Na and density with Cl (Fig. 2) establish that Na and Cl behave conservatively with respect to mixing of seawater and brine at the interface. It follows that a linear mixing plot of some other element versus either Na or Cl signifies conservative behavior of that element, whereas positive or negative deviations from linearity must be caused by release, respectively removal at the corresponding depth. This is illustrated in Fig. 3 for the heavier alkali

elements, K and Rb. Profiles show their concentrations rising from seawater values at about 2150 m to slightly higher levels at 2220 m and then much more rapidly across the interface to the top of the brine. Below about 2250 m the brine is homogeneous, within analytical uncertainties, at concentrations that are ~70% higher than in seawater for K and ~50% for Rb. While their profiles display no manifest signs of non-conservative behavior, their mixing plots versus Na say otherwise (Fig. 3). K and Rb are linearly correlated with Na throughout the entire transition from seawater to brine, except for the two points labeled with closed symbols. The same points are labeled in the profiles as a reminder that they represent the steepest part of the pycnocline, at 2235 and 2240 m. The Rb data in particular, being somewhat more accurate, show convincingly that the correlations encompass most of the concentration gradients and that the cation removal uncovered by the distinct negative deviations from linearity is confined to the depth interval 2220–2250 m. As Fig. 1 indicates, this is precisely the depth interval that harbors the two dense particle layers.

The alkaline earth elements are chemically more reactive and their behaviors are consequently more diverse (Fig. 4). Ca and Sr profiles resemble those of K and Rb, with concentrations in the brine higher than in seawater by factors of approximately 2.5 and 1.4, respectively. The Mg gradient at the interface is reversed and Mg concentrations in the brine are ~20% lower than in seawater. Its concentrations at 2235 and 2240 m are lower still, producing a local minimum and making Mg the only cation besides Ba for which evidence of non-conservative behavior is plainly visible in its profile. Ba, whose behavior at the interface and within the brine is affected by redox processes and barite solubility, will be discussed later. The Sr–Na mixing plot (Fig. 5), like K–Na and Rb–Na, displays removal at 2235 and 2240 m. Despite the inverse slope of the linear correlation, this also holds true for Mg and its removal seems especially strong. In sharp contrast, the Ca–Na

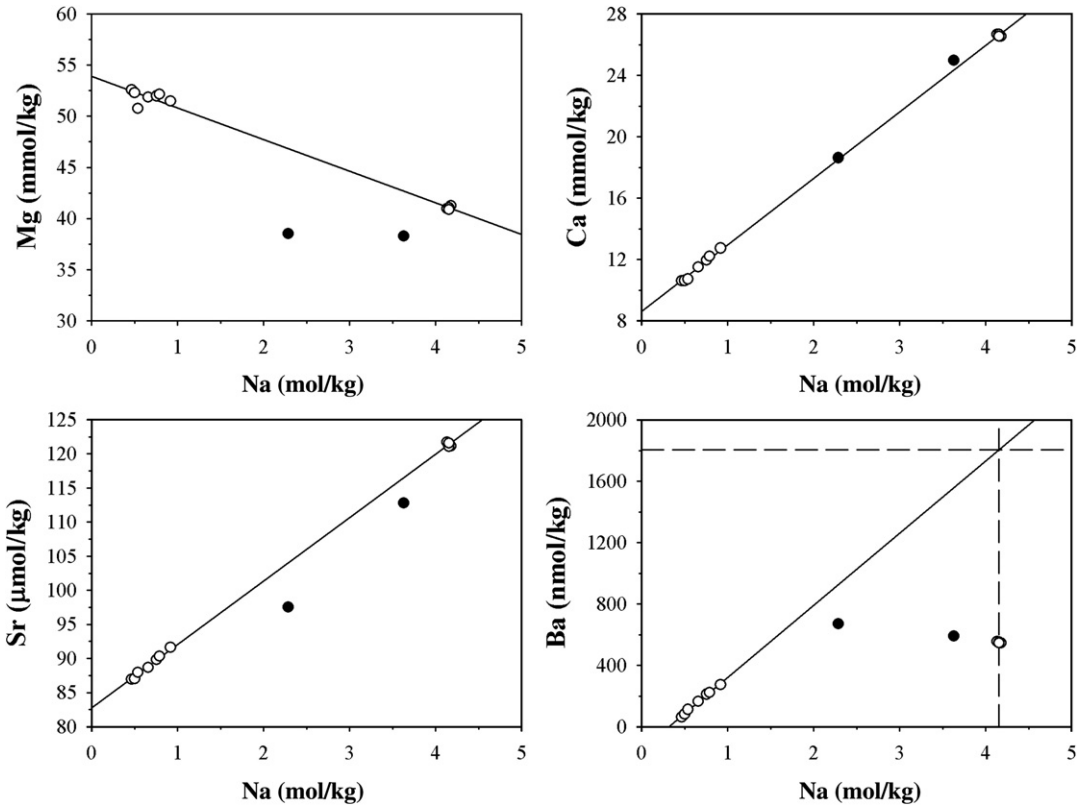

Fig. 5. Mixing plots (Mg–Na, Ca–Na, Sr–Na, Ba–Na) for the alkaline earth elements in Fig. 4. Closed symbols mark the same samples as in Fig. 2. Linear regressions are through the open symbols only, while for Ba the fit is further restricted to data above the seawater–brine interface. Note the anomalous behavior of Ca and Ba. The latter is caused by barite ($BaSO_4$) precipitation at and below the seawater–brine interface. Dashed lines indicate the extrapolated ('conservative') Ba concentration of the brine (~1800 nmol/kg).

correlation is completely linear, disregarding a small Ca excess at 2240 m.

Strong removal of elements with low polarizing power (i.e., low charge and a relatively large ionic radius), such as Rb, is rare but not unprecedented. Based on mixing plots versus salinity, James and Palmer (2000) reported Rb and Cs removal in the Ganges–Brahmaputra estuary amounting to at least 20% of the riverine flux. The removal of K is more surprising and typically associated with early diagenesis of marine sediments or seawater alteration of volcanic material (Gieskes, 1975; De Carlo, 1992). James and Palmer (2000) found no significant K removal in their estuarine samples, while K was shown to behave conservatively across the seawater–brine interface of the Red Sea deeps (Craig, 1969) as well as the Bannock Basin (de Lange et al., 1990c). Neither of the latter two publications contains Rb data. One process that has been implicated in K removal is the precipitation or reconstitution of clay minerals in anoxic sediments in the presence of silica, iron oxide, and organic matter (Mackenzie et al., 1981; Michalopoulos and Aller, 1995). Aptly called "reverse weathering", these reactions appear to produce mica-type clays and acidity, while consuming alkalinity and other ions along with K^+, for instance Na^+, Mg^{2+}, Fe^{2+}, and F^-. Although conditions at the Orca Basin interface would favor reverse weathering, key data needed to assess its importance, such as Al and silicate profiles, or the mineralogical composition of the particle layers, are not presently available. It will be demonstrated below that the prime removal process at the Orca Basin interface is about equally efficient for all alkali and alkaline earth elements, which argues against reverse weathering playing a dominant role.

Even more curious is the apparent lack of Ca removal, in light of the substantial removal of the lighter and heavier alkaline earths, Mg and Sr. A process that could remove both Mg and Sr, but leave Ca unaffected, is difficult to envisage. It is likelier that Ca removal, mimicking that of Mg and Sr, is offset by Ca release via a separate process operating at the same depths. That these two processes would cancel to yield zero net Ca removal is fortuitous, but not impossible. One process that comes to mind is dolomitization of calcium carbonate, which removes Mg and releases Ca. It should be emphasized that authigenic dolomite precipitation, which consumes both Mg and Ca, does not fit the data, since it would enhance Ca removal rather than counter it. Dolomitization has been suggested to occur in the Red Sea brines (Brooks et al., 1969), yet this was contradicted by Craig (1969) who pointed out that the expected concomitant oxygen isotope shift is not observed. In Bannock Basin, dolomitization is believed to partially sustain the compositional difference of two brine layers and to be especially active at the interface between them (de Lange et al., 1990a,b) although, unlike the present case, the absence of a particle layer makes it hard to explain its prevalence at that particular depth.

It is instructive to attempt a simple mass balance, which admittedly is poorly constrained and mainly serves to elucidate how the proposed mechanism can result in the correct non-conservative behavior, but is not meant to give a numerically accurate picture of what actually happens. I start off with two independent processes operating concurrently: dolomitization, which removes Mg, releases Ca and Sr, but does not affect K and Rb (Schijf and Byrne, 2007), plus an unspecified adsorption or ion-exchange process that removes all alkali and alkaline earth elements (including Na, even if this is not discernable within analytical uncertainty). As both processes operate only at the interface (Figs. 3 and 5) they must be related to the dense layers of particles trapped by the pycnocline (Fig. 1), acting as a source of calcium carbonate to one process and as a source of reactive surfaces to the other. A generic mass balance can now be written for Mg and Ca:

$$[\mathrm{Mg}]_{\mathrm{def}} = [\mathrm{Mg}]_{\mathrm{ads}} + [\mathrm{Mg}]_{\mathrm{dol}} \tag{2a}$$

$$[\mathrm{Ca}]_{\mathrm{def}} = [\mathrm{Ca}]_{\mathrm{ads}} - [\mathrm{Ca}]_{\mathrm{dol}} \tag{2b}$$

where the subscripts "def", "ads", and "dol", refer to total deficiencies and the contributions of adsorption and dolomitization, respectively. Concentrations, indicated by brackets, have a positive sign and the ideal stoichiometry of dolomitization imposes the constraint $[\mathrm{Mg}]_{\mathrm{dol}}=[\mathrm{Ca}]_{\mathrm{dol}}$. A mass balance identical to Eq. (2b) can be written for Sr. For K and Rb, $[\mathrm{X}]_{\mathrm{def}}=[\mathrm{X}]_{\mathrm{ads}}$ (X is any element). Deficiencies, $[\mathrm{X}]_{\mathrm{def}}$, were quantified by subtracting measured concentrations, $[\mathrm{X}]_{\mathrm{M}}$, from 'conservative' concentrations, $[\mathrm{X}]_{\mathrm{T}}$, estimated using the linear correlations in Figs. 3 and 5, and the Na concentrations in Table 2. They are listed in Table 4.

Unfortunately, the mass balances for Mg, Ca, and Sr cannot be simultaneously solved unless further assumptions are made about the removal process. Absent any knowledge about the nature of the adsorbing surface, estimates of relative reactivities can be based solely on cation chemical properties. Sverjensky (2006) showed that solid/solution distribution coefficients, K_d, of alkaline earth elements increase or decrease with their ionic radius, r, depending on the dielectric constant of the adsorbing surface. If this is also true for the alkali

Table 4
Simultaneous solution of mass balance equations for the alkaline earth elements, except Ba

X	2235 m					2240 m				
	$[X]_T$ [a]	$[X]_{def}$	$[X]_{ads}$	$[X]_{dol}$	$[X]_{ads}/[X]_T$ (%)	$[X]_T$ [a]	$[X]_{def}$	$[X]_{ads}$	$[X]_{dol}$	$[X]_{ads}/[X]_T$ (%)
K^+	13.9	1.5	1.5	0 [b]	11	16.5	1.4	1.4	0[b]	8
Rb^+	1.62	0.13	0.13	0[b]	8	1.85	0.09	0.09	0[b]	5
Mg^{2+}	46.8	8.3	6.6	1.7	14	42.7	4.4	2.5	1.9	6
Ca^{2+}	18.5	−0.1 [c]	1.6	1.7	8	24.3	−0.6[c]	1.3	1.9	5
Sr^{2+}	104	6.5	8.2	1.7	8	116	3.7	5.6	1.9	5

Two independent processes are considered, adsorption and dolomitization, operating at 2235 m and 2240 m only. [X] is the concentration of element X in μmol/kg (Rb and Sr) or mmol/kg (others). Subscripts "def", "ads", and "dol" refer to deficiencies with respect to $[X]_T$ and the contributions of adsorption and dolomitization, respectively. The ideal stoichiometry of dolomitization imposes the constraint $[Mg]_{dol}=[Ca]_{dol}$. See text for details.

[a] Estimated from the linear correlations in Figs. 3 and 5, and the Na concentrations in Table 2.

[b] K and Rb are assumed to be unaffected by dolomitization.

[c] Negative concentrations indicate a slight Ca excess.

elements then stronger K than Rb adsorption points to a surface with a low dielectric constant, like amorphous Fe, Al, or Si oxides. Sverjensky (2006) argued that $\log K_d \propto 1/r$, where $K_d \approx [X]_{ads}/[X]_M$ under the current definition. According to Robinson and Stokes (1959), Ca^{2+} and Sr^{2+} have identical Stokes radii so it is reasonable to pose $[Ca]_{ads}/[Ca]_M \approx [Sr]_{ads}/[Sr]_M$, with $[Ca]_M$ and $[Sr]_M$ taken from Table 2. I will moreover assume that relative amounts of Sr and Ca released during dolomitization reflect the Sr/Ca ratio of foraminiferal calcite i.e., $[Sr]_{dol}/[Ca]_{dol} \approx 1$ mmol/mol. These two supplementary constraints lead to the solution in Table 4.

While this solution may not be truly quantitative, its qualitative characteristics appear to be robust and can be meaningfully interpreted. Like K and Rb, alkaline earth element adsorption comprises around 10% of $[X]_T$ at 2235 m and roughly half as much at 2240 m. This is supported by the observation that the particle layer at 2235 m has greater optical density (Fig. 1), keeping in mind that there may be compositional differences between the layers as indicated by large color variations of the filtered material. The amount of dolomite formed at each depth is approximately the same, ~2 mmol/kg. Whereas the assumption $[Sr]_{dol}/[Ca]_{dol} \approx 1$ mmol/mol may seem arbitrary, the results in Table 4 are not very sensitive to this number. When $[Sr]_{dol}=0$, the amount of dolomite formed is only slightly smaller and the results barely change. When $[Sr]_{dol}/[Ca]_{dol} \approx 3$ mmol/mol, the Mg deficiency is entirely accounted for by dolomitization and the reactivity of Mg with respect to adsorption becomes unrealistically low. Sr/Ca ratios of planktonic foraminifera fall in the range 1–2 mmol/mol (Harding et al., 2006). If all Sr is released during dolomitization (a worst case scenario) then $[Sr]_{dol}/[Ca]_{dol}$ is exactly twice that ratio. Planktonic foraminifera are a primary constituent of the >63-μm fraction of Orca Basin sediments (Tompkins and Shephard, 1979) and should therefore be abundant in the particle layers as well. Nevertheless, it is important to acknowledge that the model does not consider (i) dolomitization of aragonite (e.g., pteropods), which has a higher Sr/Ca ratio than calcite (Katz et al., 1972); (ii) calcium carbonate dissolution; and (iii) partial or non-ideal dolomitization. Without additional information, the solution presented here is little more than an example. Such information could be obtained from chemical analysis of the particulate matter. However, measuring concentrations of adsorbed alkali and alkaline earth cations is daunting because of the copious salt residue left behind after filtering the brine samples and the lability of the adsorbed fraction which foils any strategy to selectively remove this salt.

4.3. Composition of the Louann Salt: a probable source of the Orca Basin brine

Underneath the northern part of the Gulf of Mexico and the southern coastal United States lies an evaporite deposit of Jurassic age known as the Louann Salt, the largest on Earth (Land et al., 1995). Several lines of evidence, offered by various investigators, suggest that the Louann Salt is the most likely source of the Orca Basin brine. Observations supporting this hypothesis include the topography of the northern Gulf of Mexico continental shelf, which is indicative of active and widespread salt diapirism (Trabant and Presley, 1978), seismic bottom surveys that reveal seafloor exposure of salt in the vicinity of Orca Basin (Addy and Behrens, 1980), and the visual presence of a 'brine river' flowing into Orca Basin from the upper slope (Brooks et al., 1990). Trabant and Presley (1978) claimed that the bromide (Br^-) concentration of the brine (80 ppm) is consistent with the dissolution of 308 g of halite from

the Louann Salt per liter of seawater. Their calculation (also cited in the review by Sheu, 1990) is clearly erroneous, as it implies that the Br^- concentration of the mixture is greater than that of the two end members, seawater (~65 ppm) and salt (taken as 34–51 ppm). The error appears to have been caused by failure to account for the density of the mixture. Sheu et al. (1988) demonstrated that simultaneously solving mass balances for $\delta^{34}S$ and $\delta^{18}O$ in the brine correctly predicts sulfate isotopic ratios in the Louann Salt, but they did not explicitly discuss its concentration. Craig (1969) derived the composition of a hypothetical salt that, when dissolved in 1 kg of seawater, would yield the measured concentrations of a large number of major, minor, and trace elements in the Red Sea brines, and showed it to be very close to that of the Louann Salt near the halite–sylvite transition.

Following the approach of Craig (1969), I have tried to consolidate some of these arguments by determining the amount and composition of an 'ideal' halite that faithfully recreates the Orca Basin brine when dissolved in 1 kg of seawater. I will refer to it as "Ideal Orca Basin Halite", hereafter abbreviated as IOBH. A simple mass balance was applied to solutes that can reasonably be expected to behave conservatively and for which the requisite data are available. These are the alkali elements Na, K, and Rb, the alkaline earth elements Mg, Ca, and Sr, and the anions chloride, sulfate, bromide, and iodide. For iodide the total dissolved iodine concentration (I_T) was used, which behaves conservatively despite a variable solution speciation between oxidized (IO_3^-) and reduced (I^-) forms (Byrne, 2002). Seawater concentrations were taken from Byrne (2002), except I_T, for which the average concentration in seawater overlying the Orca Basin was taken from Wong et al. (1985). The composition of the Orca Basin brine is given in Table 3 and compared with previous measurements by three research groups, spanning two decades. Dismissing the anomalous sulfate concentration of Van Cappellen et al. (1998), agreement is very good with only minor deviations in either direction. As mentioned before, the slightly elevated concentration of K may be analytical and due to Na interference. Concentrations of Br^- and I_T in the brine were taken from Trabant and Presley (1978) and Wong et al. (1985), respectively. All seawater and brine concentrations were converted to ppm and are listed in Table 5.

The composition of IOBH can now be calculated from the following equation:

$$C_{salt} = C_{brine}\left(\frac{w_{seaw}}{w_{salt}} + 1\right) - C_{seaw}\frac{w_{seaw}}{w_{salt}} \quad (3)$$

where C are concentrations (in ppm), w are masses (in grams), and subscripts refer to the various components in the mixture. By performing the calculation on a

Table 5
Composition of the Ideal Orca Basin Halite (IOBH)

Element	Eq. (3) (281 g of salt per kg of seawater)				Louann Salt[a]		
	Seawater[b]	Brine[c]	Mixture	IOBH	All halite	Early+main halite	Halite–bittern transition
Na^+ (%)	1.08	9.55	9.47	39.3	–	–	–
Cl^- (%)	1.95	14.7	14.8	60.7	–	–	–
K^+	399	684		1700	300	200 (200–300)	3100 (200–63,300)
Mg^{2+}	1280	997	1022	91[†]	91	85 (67–905)	540 (84–2770)
Ca^{2+}	417	1070		3377	3300	3550 (10–106,000)	2400 (10–23,100)
SO_4^{2-}	2710	3720		7307	6450	7450 (40–174,200)	4650 (1000–56,600)
Rb^+	0.12	0.17		0.3	0.04[d]	0.02 (0.01–0.1)[d]	0.3[d](h), 45[d](s)
Sr^{2+}	7.8	10.7		21	15	15 (5–294)	15 (10–90)
					9[d]	7 (1–21)[d]	13[d](h), 1.6[d](s)
Br^-	67	80[f]		126	180	180 (20–2150); 50[e]	180 (20–410); 218[e]
					170[d]	188 (29–277)[d]	107[d](h), 1357[d](s)
I_T	0.05[g]	0.5[g]		2.1	1.9	2.0 (0.1–6.9)	1.5 (0.1–9.1)

The median composition of the Louann Salt (with ranges in parentheses) is given for samples from the halite zone and near or inside the bittern zone (Grand Saline Dome and others). Concentrations in ppm, unless otherwise indicated. A simple mass balance was used to calculate the composition of an ideal halite ("IOBH") that would yield a solution with the average composition of the Orca Basin brine if 281 g of it were dissolved in 1 kg of seawater. The Na and Cl abundances of IOBH are based on pure halite, not accounting for the contributions of minor components. Sources: [a] Kreitler and Muehlberger (1981), unless otherwise indicated. Halite–bittern transition corresponds to their "edge of dome" samples; [b] Byrne (2002), unless otherwise indicated; [c] this work, unless otherwise indicated; [d] Land et al. (1988, 1995), h = halite, s = sylvite; [e] Land et al. (1988), reanalysis of some of the original samples of Kreitler and Muehlberger (1981); [f] Trabant and Presley (1978); g Wong et al. (1985), I_T = total dissolved iodine concentration.

[†]Eq. (3) yields a Mg abundance of −24 ppm (see text).

mass basis, the significant change in density upon dissolution of the salt need not be accounted for. First, the value of w_{salt} was determined as the amount of pure halite (NaCl) that best reproduces the concentrations of both Na and Cl in the brine (using $w_{seaw}=1000$ g) and found to be 281 g. With this result, C_{salt} was then calculated from Eq. (3) for each of the minor components, using the data in Table 5. Although the IOBH abundances of some minor components approach 1%, its Na and Cl abundances were not adjusted for these contributions.

One of the most comprehensive analyses of the Louann Salt was reported by Kreitler and Muehlberger (1981), who measured abundances of K, Mg, Ca, Sr, Cl, Br, I, and sulfate, as well as Fe and Mn, in a large number of samples from Grand Saline Dome representing a transect from early ($CaSO_4$-rich) halite, through the main halite zone, up to the onset of bittern deposition. Data are summarized in Table 5 for the entire transect and separately for the early+main halite and late halite zones ("edge of dome"; their Table 15). Since the variance among samples is high, even within each zone, data are presented as median values and ranges. Also given are Rb, Sr, and Br concentrations for the main halite zone and for the bittern zone (halite and sylvite) in salt domes from Texas to Alabama (Land et al., 1988, 1995). Kreitler later reanalyzed some of their original samples and apparently found them to be lower in Br (Land et al., 1988), but the older data are actually in better agreement with the data of Land et al. (1995) (but not with those cited by Trabant and Presley, 1978).

Considering the conceptual simplicity of this model, the agreement between the compositions of IOBH and the Louann Salt for all minor components is remarkable (Table 5). One exception is the abundance of Mg which is poorly constrained, whereby Eq. (3) yields $C_{salt}=-24$ ppm. However, substituting the median Louann Salt Mg abundance into Eq. (3) yields $C_{brine}=1022$ ppm, which is only ~3% higher than the measured concentration (Table 5). While the IOBH composition matches the average Louann Salt composition quite well, there are some exceptions. The K and Rb abundances of IOBH substantially exceed the ranges reported for the early+main halite zone and fall squarely within the halite–bittern transition. In contrast, slightly elevated Ca and sulfate abundances, and a low Mg abundance seem to fit better within the early+main halites, although in these cases the IOBH abundances fall within the reported ranges of either zone, which are broad. Measurements of Sr, Br, and iodine abundances in the Louann Salt are widely scattered and the ranges of the two zones are nearly identical, making it difficult to ascribe the IOBH composition to one or the other.

It has emerged from the investigations of Land et al. (1988, 1995) that the geochemistry of the Louann Salt is elaborate and a major challenge to interpret. Land et al. (1988, 1995) showed that certain details of its composition do not conform to the sequence of primary mineral facies deposited along the evaporation path of seawater established, for instance, by McCaffrey et al. (1987). Seawater diagenesis can transform carnallite to halite+sylvite, preferentially mobilizing elements like K, Rb, and Sr, which may then become segregated by precipitation of secondary minerals or by recrystallization of primary minerals in the resulting formation waters. In addition, these formation waters can be encapsulated in the modified facies as fluid inclusions (Land et al., 1995). Some of these transformations are unique to the Louann Salt, which makes the congruent composition of IOBH all the more significant (Table 5). What can surely be said, based on these results, is that the Orca Basin brine appears to have been formed by seawater dissolution of Louann Salt from the halite–bittern transition, possibly modified by prior seawater diagenesis, with little or no subsequent chemical evolution. This conclusion is essentially the same as the one reached by Craig (1969) for the Red Sea brines. The low Mg concentration and slightly elevated Ca and sulfate (and Sr?) concentrations of the Orca Basin brine could be attributed to minor dolomitization and dissolution of (secondary) anhydrite or gypsum, but the current data do not really justify such a refinement. Some of these issues might be resolved with further studies of elements that are more diagnostic of the source minerals and diagenetic processes involved.

4.4. Barium and sulfate concentrations and the solubility of barite

One of the most puzzling aspects of Orca Basin geochemistry is the lack of free sulfide in the brine, in spite of its anoxia and the profiles and speciations of various redox-sensitive elements, like iodine (Wong et al., 1985) and selenium (Takayanagi and Wong, 1985), which give ample proof of its low redox potential. It has been argued that hypersaline waters are hostile to sulfate-reducing bacteria (Wiesenburg et al., 1985), but this idea is at odds with the recent description of diverse and thriving bacterial communities in the eastern Mediterranean brines, whose chloride concentrations of up to ~10 M are, if anything, less hospitable. Bacterial cell counts and metabolic activity were found to rival those in the overlying seawater and sulfide

production rates of up to 80 μM per day were measured (van der Wielen et al., 2006), accounting for the more than thousandfold higher sulfide concentrations (1–16 mM) in these brines, notwithstanding their similar age. The most commonly accepted answer to this problem is scavenging of free sulfide from the Orca Basin brine by precipitation with dissolved Fe(II), which is extremely abundant. This is illustrated in Fig. 6, which juxtaposes Fe(II) and H_2S profiles in the Orca and Bannock Basins. The profiles are strikingly reversed in terms of both shapes and relative concentrations. In the Bannock Basin brine, sulfide production is vigorous and buffers the concentration of Fe(II), which is mainly produced by reductive dissolution at the interface but rapidly removed below due to iron sulfide precipitation. The opposite seems to happen in Orca Basin: strong production of Fe(II) keeps free sulfide in the brine at trace levels (<1 μM). Studies of carbon and sulfur budgets and isotopic compositions (Sackett et al., 1979; Sheu and Presley, 1986b; Sheu et al., 1988) indicate that most sulfate reduction in Orca Basin takes place at the seawater–brine interface and in the sediments, whereas net sulfide production within the brine itself is low. Sulfide production in the brine is clearly not sulfate-limited, although Sheu and Presley (1986b) have suggested that it may be carbon-limited in the sediments. The source of Fe(II) in the Orca Basin is still a topic of debate. It may be associated either with the unusual mode of brine emplacement, or with frequent slumps constituting a steady supply of Fe(III)-rich shelf sediments (Tompkins and Shephard, 1979; Addy and Behrens, 1980). Similar mechanisms of Fe enrichment have been proposed for the abyssal Black Sea, invoking lateral transport of both lithogenous Fe from shelf sediments and an uncoupled source of reactive Fe diagenetically mobilized on the continental margins (Anderson and Raiswell, 2004; Raiswell and Anderson, 2005).

The aforementioned observations are also in agreement with the study of LaRock et al. (1979) who found evidence for active bacterial communities above the seawater–brine interface and on the seafloor, but fewer within the brine. Part of the sulfide produced at the interface seems to escape precipitation by upward diffusion into a layer where Fe(II) concentrations are low and some oxygen is available. The sulfate profile in Fig. 7 has a minor but distinct maximum at the steepest part of the pycnocline. The SO_4–Cl mixing plot displays positive deviations from linearity at the depths coinciding with two particle layers, the greatest sulfate excess being associated with the upper, denser one (Fig. 1). Mass balance calculations for sulfate $\delta^{34}S$ and $\delta^{18}O$, performed by Sheu et al. (1988), demonstrated that sulfide is oxidized to sulfate at the top of the brine. Putting all this together, it is likely that the bacteria alluded to by LaRock et al. (1979), at least some of which may be chemoautotrophic sulfide oxidizers, reside in the dense particle layers and are responsible for the sulfide oxidation causing the sulfate excess at 2235 and 2240 m.

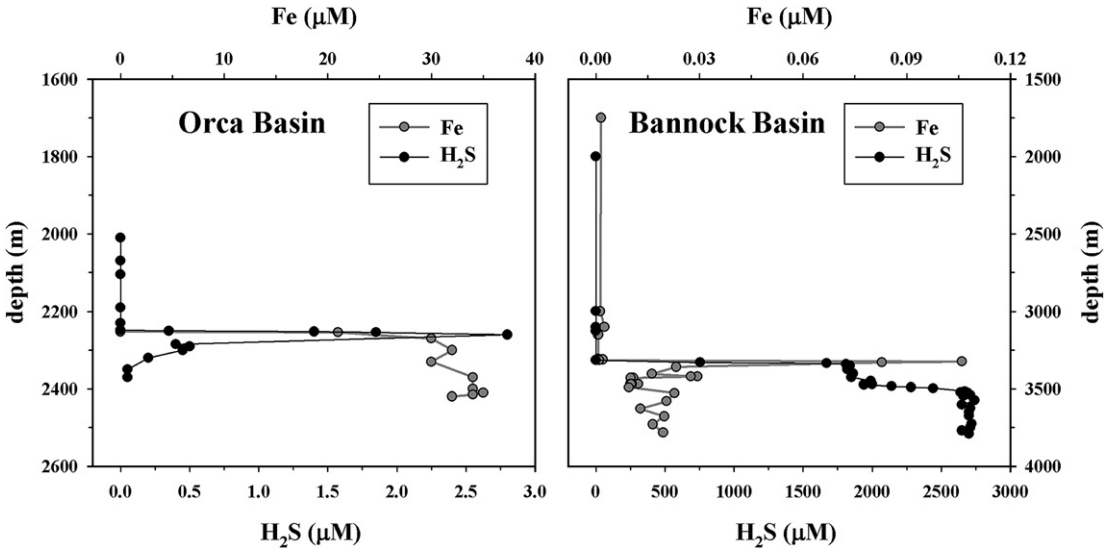

Fig. 6. Dissolved H_2S and total dissolved Fe in Orca Basin and Bannock Basin. Note the strikingly interchanged profiles in terms of both shapes and relative concentrations. Orca Basin profiles after Wiesenburg et al. (1985). Bannock Basin H_2S data from Luther et al. (1990) and Fe data from Saager et al. (1993).

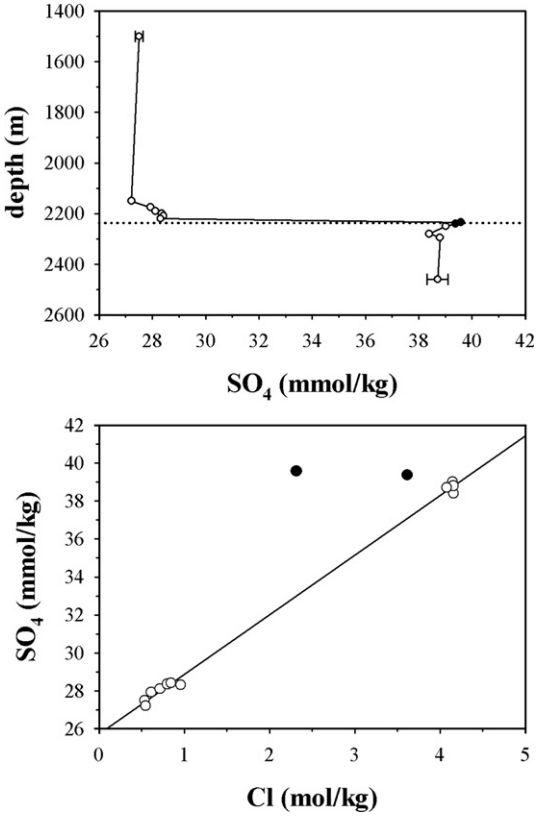

Fig. 7. Profile of dissolved sulfate (SO_4) and the corresponding SO_4–Cl mixing plot. Error bars on the shallowest and deepest samples are representative of analytical uncertainties for the seawater and brine samples, respectively. Horizontal dotted line indicates the steepest part of the pycnocline. Closed symbols mark the same samples as in Fig. 2. Linear regression is through the open symbols only. Note the opposite behavior at the seawater–brine interface with respect to some of the alkali and alkaline earth elements.

The sulfate profile in Fig. 7 also shows that concentrations in the brine are about 40% higher than in seawater and the results in Table 5 suggest that most of this sulfate is traceable to the Louann Salt. High sulfate concentrations can initiate precipitation of poorly soluble alkaline earth sulfates. For example, authigenic gypsum ($CaSO_4 \cdot 2H_2O$) composites as large as 0.5 m across have been dredged from the Bannock Basin (Scientific staff of Cruise *Bannock* 1984-12, 1985). The sulfate salts of Sr (celestite) and Ba (barite) are even less soluble than gypsum, yet calculating their degrees of saturation in mixed electrolyte solutions with ionic strengths as high as 6–7 *m* remains challenging. Krumgalz et al. (1999) used the Pitzer formalism to estimate degrees of saturation for alkaline earth sulfates and other salts in the brines of Orca Basin, Tyro Basin, and Bannock Basin below interface I/II (de Lange et al., 1990b). They found the Tyro Basin brine to be supersaturated with respect to celestite, Bannock Basin brine II with respect to barite, and both brines to be near saturation for all other alkaline earth sulfates. The Orca Basin brine was found to be significantly undersaturated with respect to both gypsum and anhydrite ($CaSO_4$), but no data were available at that time to do calculations for Sr and Ba.

Rb is one of the last elements to precipitate during evaporation of seawater, preferentially concentrating in carnallite at levels up to ~300 ppm by weight (Holser, 1979). It should therefore not be surprising that the Rb profile in Fig. 3 shows no signs of removal within the brine. Although the same can be said for the Sr profile (Fig. 4), the findings of Krumgalz et al. (1999) indicate that the degree of celestite saturation is not as clear-cut. In the Ba profile, however, and in the Ba–Na mixing plot (Fig. 5) signs of Ba precipitation (probably as barite) are unmistakable. Ba concentrations first increase to a maximum of 670 nmol/kg at 2235 m, but decrease below the interface to an average concentration of 549 nmol/kg in the brine (Table 2). The new Sr and Ba data in Table 3 allow degrees of saturation at ambient pressure, $\Omega_{MX}(P)$, to be calculated for conditions near the top of the brine (P=230 bar). The results are $\Omega_{MX}(P)$=0.404 for celestite and $\Omega_{MX}(P)$=1.47 for barite at T=25 °C (B.S. Krumgalz, pers. comm.) i.e., Sr is undersaturated by about 60% and Ba supersaturated by about 50%, supporting my conclusions (Figs. 4 and 5). In reality the brine is colder (T=5.6 °C) and these values represent lower limits, but the effect of temperature in this range is comparatively small (Rushdi et al., 2000).

By extrapolating the linear regression in the Ba–Na mixing plot (Fig. 5) to the appropriate Na concentration, the amount of Ba the brine would contain if Ba were behaving conservatively can be estimated. The resulting Ba concentration (1804 nmol/kg) is more than three times higher than the one actually measured (Table 3). The effect of barite precipitation becomes even more apparent if the Ba profile is compared with those of several conservative elements on a common concentration scale. This is done in Fig. 8, where concentrations in seawater and in the brine were assigned values of 0 and 1, and all intermediate concentrations were scaled proportionally. The virtually identical scaled profiles of Na, Rb, and Sr indicate that these cations indeed behave conservatively, showing no sign of precipitation within the brine. The scaled Ba profile confirms that the measured concentration in the brine is less than 30% of what it would be if Ba behaved conservatively. At the interface, in addition to barite precipitation, Ba concentrations may be affected by adsorption and dolomitization in much the same way as Sr.

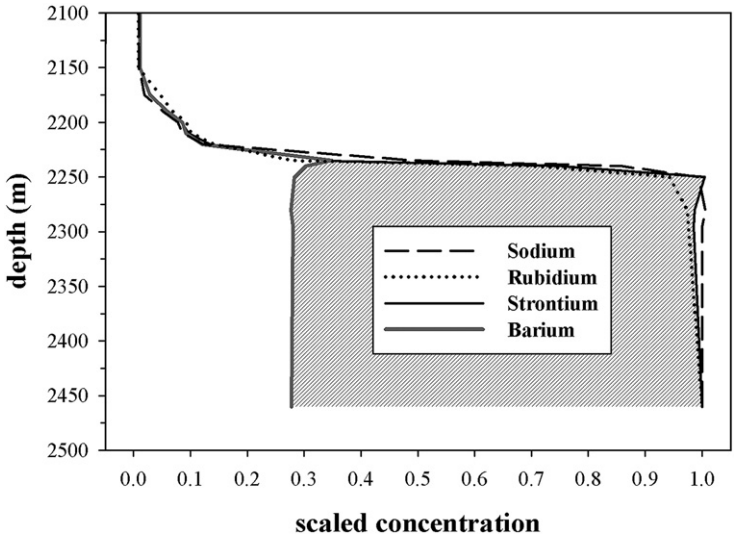

Fig. 8. Scaled concentrations (C_s) of Na, Rb, Sr, and Ba, where $C_s=(C_z-C_{1500})/(C_{2460}-C_{1500})$ and z is depth. Detail of the brine emphasizes the anomalous behavior of Ba. Ba concentrations were scaled by setting C_{2460}(Ba)=1804 nmol/kg, which is the 'conservative' Ba concentration derived by extrapolating the linear regression in the Ba–Na mixing plot to the Na concentration of the brine (Fig. 5). The shaded area is the amount of Ba missing relative to how much would be there if Ba were behaving conservatively.

If the estimated 'conservative' Ba concentration is substituted for C_{brine} in Eq. (3) and the Ba concentration at 1500 m is used for C_{seaw}, the Ba abundance of IOBH is about 1 ppm. Based on his calculations for the Red Sea brines (Ba ~6.6 μmol/kg), Craig (1969) determined the Ba abundance of their hypothetical halite source to be 3.9 ppm. There are few published analyses of Ba abundances in evaporite halite facies and apparently none for the Louann Salt. Shepherd and Chenery (1995) measured Ba/Sr ratios (w/w) in fluid inclusions of the Triassic Wilkesley Halite and arrived at a median value of ~0.05 for the upper halite unit. Leslie et al. (1997) found high Ba abundances in laminated anhydrites of the Permian Castile Formation, as might be expected for sulfate mineral separates, but a median Ba/Sr ratio of ~0.02. The hypothetical halite source of the Red Sea brines (Craig, 1969) also has a Ba/Sr ratio of ~0.02. Ba and Sr may segregate into alternate minerals during seawater evaporation and subsequent diagenesis of the resulting evaporites. Still, the IOBH Ba/Sr ratio of 1/21 ≈ 0.05 (Table 5) appears to be the right order of magnitude.

5. Summary

In this work I have presented detailed profiles of density and the major seawater cations and anions from the deep Gulf of Mexico into the anoxic Orca Basin brine, across the seawater–brine interface. In addition, I have presented profiles of Rb, Sr, and Ba concentrations, measured for the first time by ICP-MS. This study has yielded the following insights:

1) Na plus Cl make up more than 95% of the average brine composition and dominate its density, which is about 20% higher than that of the overlying seawater. Whereas a detailed explanation of the asymmetrical shape of the density profile at the interface awaits further study, the pronounced pycnocline at 2235–2240 m is an extremely stable feature ensuring the longevity and persistent anoxia of the brine while acting as an efficient particle trap. Dense particle layers at the interface are prominently visible in light transmission profiles.
2) These dense particle layers are associated with non-conservative behavior of all cations, except Na, Cl, and Ca. An unspecified adsorption or ion-exchange process appears to remove about 5–10% of their concentrations predicted from linear mixing plots versus Na. Ca adsorption may be negated by Ca release during dolomitization, which enhances Mg removal, explaining the Mg minimum at the interface. Simultaneous solution of the mass balance equations for Ca, Mg, and Sr called for a proportional release of Sr and Ca equal to their ratio in foraminiferal calcite, which could be an important fraction of the calcium carbonate converted in the dolomitization process.

3) Different mass balance calculations show that dissolution of about 281 g of late stage halites from the Louann Salt per kg of seawater would reproduce the Orca Basin brine largely as it exists today. No secondary processes are required to account for its composition. Elevated K and Rb concentrations may be due to enrichments of these elements in the late stage halites by prior diagenetic modification of bittern facies in contact with seawater.
4) Unlike Ca and Sr, Ba shows evidence of removal in the brine, namely a maximum at the interface and sharply decreasing concentrations below to levels that are about 70% lower than what is predicted from a linear Ba–Na mixing plot. Thermodynamic calculations suggest that Sr is significantly undersaturated with respect to celestite ($SrSO_4$) and that Ba is oversaturated with respect to barite ($BaSO_4$) by about 50%. Ba concentrations in the brine are thus buffered by authigenic barite precipitation. Earlier calculations had suggested that Ca is undersaturated with respect to anhydrite and gypsum. Excess sulfate is produced at the interface from sulfide diffusing upward into a layer where Fe(II) concentrations are low enough to prevent precipitation but where sufficient oxygen is present to sustain oxidation, possibly by chemoautotrophic bacteria.

Knowledge of Orca Basin geochemistry is steadily improving, yet more work remains to be done. Better constraints on the origin and history of the Orca Basin brine may be gained from Sr isotopes (e.g., Faure and Jones, 1969; de Lange et al., 1990b). An autonomous large-volume in situ filtration system was deployed in 2003 to collect sizeable quantities of particulate matter (equivalent to ~1000 L of water). Measurements of metal concentrations and metal speciation in these samples are now underway, although targeting the tenuously adsorbed alkali and alkaline earth elements may prove unfeasible in the presence of so much salt. Transition metal (Co, Ni, Cu, Zn, Cd, Pb) analyses of filtered seawater and brine are planned as well, to extend the preliminary investigations of Trefry and Presley (1977).

Acknowledgements

I am deeply grateful to the University of South Florida (USF) for the award of a New Researcher Grant, which made this work possible. David Hollander (USF, College of Marine Science) rekindled my interest in the geochemistry of marine anoxic basins by inviting me to participate in the 2003 Orca Basin cruise. Tamara Pease (University of Texas, Marine Science Institute) and Joe Werne (University of Minnesota, Large Lakes Observatory) are thanked for crucial logistical support and sharing of equipment. My wife and fellow scientist, Hali Kilbourne, assisted with sample collection. I am greatly indebted to Professor Boris Krumgalz (IsrArt Gallery, Nesher, Israel), who interrupted a well-deserved retirement to calculate mineral solubilities in the Orca Basin brine. Rob Walker (Florida Institute of Oceanography) supplied and installed the silicone internal springs for the Niskin bottles, which were indispensable for trace metal-free sampling. Captain, crew, and scientific party of the R/V *Longhorn* provided expert seamanship and pleasant working conditions. Kelly Quinn kindly proofread an early version of the text. The manuscript also benefited greatly from comments by Rob Raiswell and one anonymous reviewer, and from diligent editorial work by David Rickard.

References

Addy, S.K., Behrens, E.W., 1980. Time of accumulation of hypersaline anoxic brine in Orca Basin (Gulf of Mexico). Mar. Geol. 37, 241–252.

Anderson, T.F., Raiswell, R., 2004. Sources and mechanisms for the enrichment of highly reactive iron in euxinic Black Sea sediments. Am. J. Sci. 304, 203–233.

Backer, H., Schoell, M., 1972. New deeps with brines and metalliferous sediments in the Red Sea. Nature Phys. Sci. 240, 153–158.

Brewer, P.G., Spencer, D.W., 1969. A note on the chemical composition of the Red Sea brines. In: Degens, E.T., Ross, D.A. (Eds.), Hot Brines and Recent Heavy Metal Deposits in the Red Sea. A Geochemical and Geophysical Account. Springer-Verlag, New York, NY, pp. 174–179.

Brooks, R.R., Kaplan, I.R., Peterson, M.N.A., 1969. Trace element composition of Red Sea geothermal brine and interstitial water. In: Degens, E.T., Ross, D.A. (Eds.), Hot Brines and Recent Heavy Metal Deposits in the Red Sea. A Geochemical and Geophysical Account. Springer-Verlag, New York, NY, pp. 180–203.

Brooks, J.M., Wiesenburg, D.A., Roberts, H., Carney, R.S., MacDonald, I.R., Fisher, C.R., Guinasso Jr., N.L., Sager, W.W., McDonald, S.J., Burke Jr., R.A., Aharon, P., Bright, T.J., 1990. Salt, seeps and symbiosis in the Gulf of Mexico. A preliminary report of deepwater discoveries using DSV *Alvin*. Eos, Trans. - Am. Geophys. Union 71, 1772–1773.

Byrne, R.H., 2002. Speciation in seawater. In: Ure, A.M., Davidson, C.M. (Eds.), Chemical Speciation in the Environment. Blackwell Science, Oxford, UK, pp. 322–357.

Craig, H., 1969. Geochemistry and origin of the Red Sea brines. In: Degens, E.T., Ross, D.A. (Eds.), Hot Brines and Recent Heavy Metal Deposits in the Red Sea. A Geochemical and Geophysical Account. Springer-Verlag, New York, NY, pp. 208–242.

De Carlo, E.H., 1992. Geochemistry of pore water and sediments recovered from the Exmouth Plateau. In: von Rad, U., Ul Haq, B., Kidd, R.B., O'Connell, S. (Eds.), Proc. ODP Sci. Res., vol. 122. Texas A&M University (Ocean Drilling Program), College Station, TX, pp. 295–308.

de Lange, G.J., Middelburg, J.J., van der Weijden, C.H., Catalano, G., Luther III, G.W., Hydes, D.J., Woittiez, J.R.W., Klinkhammer, G.P., 1990a. Composition of anoxic hypersaline brines in the Tyro and Bannock Basins, eastern Mediterranean. Mar. Chem. 31, 63–88.

de Lange, G.J., Boelrijk, N.A.I.M., Catalano, G., Corselli, C., Klinkhammer, G.P., Middelburg, J.J., Müller, D.W., Ullman, W.J., van Gaans, P., Woittiez, J.R.W., 1990b. Sulphate-related equilibria in the hypersaline brines of the Tyro and Bannock Basins, eastern Mediterranean. Mar. Chem. 31, 89–112.

de Lange, G.J., Catalano, G., Klinkhammer, G.P., Luther III, G.W., 1990c. The interface between oxic seawater and the anoxic Bannock brine; its sharpness and the consequences for the redox-related cycling of Mn and Ba. Mar. Chem. 31, 205–217.

Faure, G., Jones, L.M., 1969. Anomalous strontium in the Red Sea brines. In: Degens, E.T., Ross, D.A. (Eds.), Hot Brines and Recent Heavy Metal Deposits in the Red Sea. A Geochemical and Geophysical Account. Springer-Verlag, New York, NY, pp. 243–250.

Gieskes, J.M., 1975. Chemistry of interstitial waters of marine sediments. Annu. Rev. Earth Planet. Sci. 3, 433–453.

Harding, D.J., Arden, J.W., Rickaby, R.E.M., 2006. A method for precise analysis of trace element/calcium ratios in carbonate samples using quadrupole inductively coupled plasma mass spectrometry. Geochem. Geophys. Geosyst. 7, Q06003. doi:10.1029/2005GC001093.

Holser, W.T., 1979. Trace elements and isotopes in evaporites. In: Burns, R.G. (Ed.), Marine Minerals Rev. Mineral., vol. 6. Mineralogical Society of America, Washington, DC, pp. 295–346.

James, R.H., Palmer, M.R., 2000. Marine geochemical cycles of the alkali elements and boron: the role of sediments. Geochim. Cosmochim. Acta 64, 3111–3122.

Jongsma, D., Fortuin, A.R., Huson, W., Troelstra, S.R., Klaver, G.T., Peters, J.M., van Harten, D., de Lange, G.J., ten Haven, L., 1983. Discovery of an anoxic basin within the Strabo Trench, eastern Mediterranean. Nature 305, 795–797.

Katz, A., Sass, E., Starinsky, A., Holland, H.D., 1972. Strontium behavior in the aragonite–calcite transformation: an experimental study at 40–98 °C. Geochim. Cosmochim. Acta 36, 481–496.

Kell, G.S., 1975. Density, thermal expansivity, and compressibility of liquid water from 0° to 150 °C: correlations and tables for atmospheric pressure and saturation reviewed and expressed on 1968 Temperature Scale. J. Chem. Eng. Data 20, 97–105.

Konovalov, S.K., Luther III, G.W., Friederich, G.E., Nuzzio, D.B., Tebo, B.M., Murray, J.W., Oguz, T., Glazer, B., Trouwborst, R.E., Clement, B., Murray, K.J., Romanov, A.S., 2003. Lateral injection of oxygen with the Bosporus plume–fingers of oxidizing potential in the Black Sea. Limnol. Oceanogr. 48, 2369–2376.

Kreitler, C.W., Muehlberger, W.R., 1981. Geochemical analyses of salt, Grand Saline Dome, East Texas. Geological Circular, 81–7. Bureau of Economic Geology, The University of Texas at Austin, pp. 188–194.

Krumgalz, B.S., Starinsky, A., Pitzer, K.S., 1999. Ion-interaction approach: pressure effect on the solubility of some minerals in submarine brines and seawater. J. Solution Chem. 28, 667–692 (Erratum: J. Sol. Chem. 32, 853–854).

Land, L.S., Kupecz, J.A., Mack, L.E., 1988. Louann Salt geochemistry (Gulf of Mexico sedimentary basin, U.S.A.): a preliminary synthesis. Chem. Geol. 74, 25–35.

Land, L.S., Eustice, R.A., Mack, L.E., Horita, J., 1995. Reactivity of evaporites during burial: an example from the Jurassic of Alabama. Geochim. Cosmochim. Acta 59, 3765–3778.

LaRock, P.A., Lauer, R.D., Schwarz, J.R., Watanabe, K.K., Wiesenburg, D.A., 1979. Microbial biomass and activity distribution in an anoxic, hypersaline basin. Appl. Environ. Microbiol. 37, 466–470.

Leslie, A.B., Harwood, G.M., Kendall, A.C., 1997. Geochemical variations within a laminated evaporite deposit: evidence for brine composition during formation of the Permian Castile Formation, Texas and New Mexico, USA. Sediment. Geol. 110, 223–235.

Li, Y.-H., Gregory, S., 1974. Diffusion of ions in sea water and in deep-sea sediments. Geochim. Cosmochim. Acta 38, 703–714.

Luther III, G.W., Catalano, G., de Lange, G.J., Woittiez, J.R.W., 1990. Reduced sulfur in the hypersaline anoxic basins of the Mediterranean Sea. Mar. Chem. 31, 137–152.

Mackenzie, F.T., Ristvet, B.L., Thorstenson, D.C., Lerman, A., Leeper, R.H., 1981. Reverse weathering and chemical mass balance in a coastal environment. In: Martin, J.-M., Burton, J.D., Eisma, D. (Eds.), River Inputs to Ocean Systems. United Nations Press, New York, NY, pp. 152–187.

McCaffrey, M.A., Lazar, B., Holland, H.D., 1987. The evaporation path of seawater and the coprecipitation of Br^- and K^+ with halite. J. Sediment. Petrol. 57, 928–937.

MEDRIFF Consortium, 1995. Three brine lakes discovered in the seafloor of the eastern Mediterranean. Eos, Trans. - Am. Geophys. Union 76, 313–318.

Michalopoulos, P., Aller, R.C., 1995. Rapid clay mineral formation in Amazon delta sediments: reverse weathering and oceanic elemental cycles. Science 270, 614–617.

Millero, F.J., Lo Surdo, A., Means, D., 1977. The density and speed of sound of Orca Basin brines. Eos, Trans. - Am. Geophys. Union 58, 1175–1176.

Millero, F.J., Lo Surdo, A., Chetirkin, P., Guinasso Jr., N.L., 1979. The density and speed of sound of Orca basin waters. Limnol. Oceanogr. 24, 218–225.

Raiswell, R., Anderson, T.F., 2005. Reactive iron enrichment in sediments deposited beneath euxinic bottom waters: constraints on supply by shelf recycling. In: McDonald, I., Boyce, A.J., Butler, I.B., Herrington, R.J., Polya, D.A. (Eds.), Mineral Deposits and Earth Evolution. Geol. Soc. London Spec. Publ., vol. 248, pp. 179–194.

Robinson, R.A., Stokes, R.H., 1959. Electrolyte Solutions. Butterworths, London, UK. 559 pp.

Rushdi, A.I., McManus, J., Collier, R.W., 2000. Marine barite and celestite saturation in seawater. Mar. Chem. 69, 19–31.

Ryan, W.B.F., Thorndike, E.M., Ewing, M., Ross, D.A., 1969. Suspended matter in the Red Sea brines and its detection by light scattering. In: Degens, E.T., Ross, D.A. (Eds.), Hot Brines and Recent Heavy Metal Deposits in the Red Sea. A Geochemical and Geophysical Account. Springer-Verlag, New York, NY, pp. 153–157.

Saager, P.M., Schijf, J., de Baar, H.J.W., 1993. Trace-metal distributions in seawater and anoxic brines in the eastern Mediterranean Sea. Geochim. Cosmochim. Acta 57, 1419–1432.

Sackett, W.M., Brooks, J.M., Bernard, B.B., Schwab, C.R., Chung, H., Parker, R.A., 1979. A carbon inventory for Orca Basin brines and sediments. Earth Planet. Sci. Lett. 44, 73–81.

Schijf, J., Byrne, R.H., 2004. Determination of $SO_4\beta1$ for yttrium and the rare earth elements at $I=0.66$ m and $t=25$ °C—implications for YREE solution speciation in sulfate-rich waters. Geochim. Cosmochim. Acta 68, 2825–2837.

Schijf, J., Byrne, R.H., 2007. Progressive dolomitization of Florida limestone recorded by alkaline earth element concentrations in saline, geothermal, submarine springs. J. Geophys. Res. 112, C01033. doi:10.1029/2006JC003659.

Schijf, J., de Baar, H.J.W., Millero, F.J., 1995. Vertical distributions and speciation of dissolved rare earth elements in the anoxic brines of Bannock Basin, eastern Mediterranean Sea. Geochim. Cosmochim. Acta 59, 3285–3299.

Scientific staff of Cruise *Bannock* 1984-12, 1985. Gypsum precipitation from cold brines in an anoxic basin in the eastern Mediterranean. Nature 314, 152−154.

Shepherd, T.J., Chenery, S.R., 1995. Laser ablation ICP-MS elemental analysis of individual fluid inclusions: an evaluation study. Geochim. Cosmochim. Acta 59, 3997–4007.

Sheu, D.D., 1990. The anoxic Orca Basin (Gulf of Mexico): geochemistry of brines and sediments. Rev. Aquat. Sci. 2, 491–507.

Sheu, D.-D., Presley, B.J., 1986a. Formation of hematite in the euxinic Orca Basin, northern Gulf of Mexico. Mar. Geol. 69, 309–321.

Sheu, D.-D., Presley, B.J., 1986b. Variations of calcium carbonate, organic carbon and iron sulfides in anoxic sediment from the Orca Basin, Gulf of Mexico. Mar. Geol. 70, 103–118.

Sheu, D.-D., Shakur, A., Pigott, J.D., Wiesenburg, D.A., Brooks, J.M., Krouse, H.R., 1988. Sulfur and oxygen isotopic compositions of dissolved sulfate in the Orca Basin: implications for origin of the high-salinity brine and oxidation of sulfides at the brine–seawater interface. Mar. Geol. 78, 303–310.

Shokes, R.F., Trabant, P.K., Presley, B.J., Reid, D.F., 1977. Anoxic, hypersaline basin in the northern Gulf of Mexico. Science 196, 1443–1446.

Sverjensky, D.A., 2006. Prediction of the speciation of alkaline earths adsorbed on mineral surfaces in salt solutions. Geochim. Cosmochim. Acta 70, 2427–2453.

Swallow, J.C., Crease, J., 1965. Hot salty water at the bottom of the Red Sea. Nature 205, 165–166.

Takayanagi, K., Wong, G.T.F., 1985. Dissolved inorganic and organic selenium in the Orca Basin. Geochim. Cosmochim. Acta 49, 539–546.

Tompkins, R.E., Shephard, L.E., 1979. Orca Basin: depositional processes, geothermal properties and clay mineralogy of Holocene sediments within an anoxic hypersaline basin, northwest Gulf of Mexico. Mar. Geol. 33, 221–238.

Trabant, P.K., Presley, B.J., 1978. Orca Basin, anoxic depression on the continental slope, Northwest Gulf of Mexico. In: Bouma, A.H., Moore, G.T., Coleman, J.M. (Eds.), Framework, Facies, and Oil-trapping Characteristics of the Upper Continental Margin. Studies in Geology. The American Association of Petroleum Geologists, Tulsa, OK, pp. 303–311.

Trefry, J.H., Presley, B.J., 1977. Transition metal chemistry of the Orca Basin. Eos, Trans. - Am. Geophys. Union 58, 1175.

Trefry, J.H., Presley, B.J., Keeney-Kennicutt, W.L., Trocine, R.P., 1984. Distribution and chemistry of manganese, iron, and suspended particulates in Orca Basin. Geo Mar. Lett. 4, 125–130.

Van Cappellen, P., Viollier, E., Roychoudhury, A., Clark, L., Ingall, E., Lowe, K., DiChristina, T., 1998. Biogeochemical cycles of manganese and iron at the oxic–anoxic transition of a stratified marine basin (Orca Basin, Gulf of Mexico). Environ. Sci. Technol. 32, 2931–2939.

van der Wielen, P.W.J.J., Bolhuis, H., Borin, S., Daffonchio, D., Corselli, C., Giuliano, L., D'Auria, G., de Lange, G.J., Huebner, A., Varnavas, S.P., Thomson, J., Tamburini, C., Marty, D., McGenity, T.J., Timmis, K.N., the BioDeep Scientific Party, 2006. The enigma of prokaryotic life in deep hypersaline anoxic basins. Science 307, 121–123.

Verplanck, P.L., Antweiler, R.C., Nordstrom, D.K., Taylor, H.E., 2001. Standard reference water samples for rare earth element determinations. Appl. Geochem. 16, 231–244.

Weast, R.C., Astle, M.J., 1982. CRC Handbook of Chemistry and Physics. CRC Press, Boca Raton, FL.

Wiesenburg, D.A., Brooks, J.M., Bernard, B.B., 1985. Biogenic hydrocarbon gases and sulfate reduction in the Orca Basin brine. Geochim. Cosmochim. Acta 49, 2069–2080.

Wong, G.T.F., Takayanagi, K., Todd, J.F., 1985. Dissolved iodine in waters overlying and in the Orca Basin, Gulf of Mexico. Mar. Chem. 17, 177–183.